nature communications

Article

https://doi.org/10.1038/s41467-025-61526-2

Ultra-soft organic combined film with piezoelectricity induced by liquid-liquid interface polar engineering

Received: 2 December 2024

Accepted: 20 June 2025

Published online: 11 July 2025

Check for updates

Yongkang Zhang[1], Xiaonan Hu[1], Zhaonan Yan[1], Siyu Zhang[1], Jiling Zhao[1], Hao Sun[1], Shuhai Liu[1,2] ✉ & Yong Qin[1,2] ✉

Although organic piezoelectric materials are increasingly being studied in the field of biomechanical sensing, the combination of high piezoelectricity and high softness is still a huge challenge due to the existence of steric hindrance effect. To conquer this, a polar engineering utilizing liquid-liquid interface induced orientation is developed. It induces polar asymmetry in two linear polymers (polystyrene-block-polyisoprene-block-polystyrene/polyethylene glycol, PEG/SIS) with low steric hindrance through a polar interface, thereby achieving high piezoelectricity in a soft material system. This PEG/SIS combined film not only exhibits a piezoelectric coefficient as high as 22.9 pC/N, and stable performance, without attenuation for 60 days, which is comparable to the piezoelectricity of the natural organic materials PVDF, but also has an ultra-softness (~1×10^{-6} Pa^{-1}) similar to that of skin, cartilage and aorta, showing high mechanical compliance with biological tissues. This work gives an approach for the development of organic piezoelectric materials, and is expected to achieve large-scale production and application of highly sensitive flexible biomechanical sensors on various surfaces and in vivo environments.

Piezoelectric materials, due to their non-centrosymmetric crystal structure, can generate piezoelectric potential under stress/strain, thereby converting mechanical stimuli into electricity. It has attracted increasing attention in biomechanical sensors for its piezoelectric response to biological motion signals such as the contraction, expansion, extrusion, and creep of biological tissues and organs[1–3]. Organic piezoelectric materials such as polyvinylidene fluoride (PVDF), polylactic acid, glycine, cellulose and collagen are the ideal choices for developing biomechanical sensing due to their inherent biocompatibility[4,5]. However, organic piezoelectric materials (e.g., PVDF with a piezoelectric coefficient d_{33} of 30 pC/N and a softness $1/E$ of 3.7×10^{-10} Pa^{-1}, evaluated by $1/E$, the inverse of Young's modulus)[6] have low piezoelectricity compared with inorganic piezoelectric ceramics such as barium titanate oxide ($BaTiO_3$, BTO) and lead zirconate titanate ($Pb(Zr, Ti)O_3$, PZT) ($d_{33} > 200$ pC/N)[7]; more importantly, their softness is several orders of magnitude lower than that of biological tissues (7×10^{-9}–2×10^{-4} Pa^{-1}) such as skin, cartilage, and muscle[8–10]. Therefore, current organic piezoelectric materials are difficult to meet the needs of biomechanical sensors for high piezoelectricity and high softness[11], which limits their practical applications.

The crucial factors depressing the piezoelectricity and softness of organic piezoelectric materials generally are derived from the steric hindrance effect[12–14]. This effect hinders the orientation of polar bonds or polar molecules under electric field polarization, and therefore suppress the piezoelectricity; it also limits the internal rotation of molecules, which leads to low softness. In order to obtain high piezoelectricity or high softness in organic piezoelectric materials, two strategies have been widely recognized and validated. The first strategy is to achieve macroscopic domain orientation of small piezoelectric molecular crystals or molecular ferroelectrics through self-assembly rather than electric field polarization, so as to avoid the size

[1]Institute of Nanoscience and Nanotechnology, School of Materials and Energy, Lanzhou University, Lanzhou, Gansu, China. [2]MIIT Key Laboratory of Complex-field Intelligent Exploration, Beijing Institute of Technology, Beijing, China. ✉e-mail: liushuhai1991@live.cn; qinyong@lzu.edu.cn

effect and the saturation effect associated with the electric field polarization[15–17]. For example, Xudong Wang's group[18] in 2021 developed a wafer-scale biomass piezoelectric glycine film via interfacial self-assembly driven by solute solubility difference. The second strategy involves piezoelectric composite that crosslinks piezoelectric materials with soft materials exhibiting small steric hindrance effect, thereby contributes to the enhanced softness of composite[19–21]. On the basis of this strategy, Gao and Hu et al.[22] in 2023 successfully synthesized elastic polymer ferroelectrics with high softness (8.3×10^{-9}–2.0×10^{-8} Pa^{-1}). The first strategy must use small piezoelectric molecular crystals or molecular ferroelectrics that intrinsically have high Young's modulus, which leads to low softness (2.5×10^{-10} Pa^{-1}); the second strategy involves crosslink that will reduce the crystallinity of piezoelectric materials, which also weakens their piezoelectricity. In general, these strategies will reduce one performance when improve another performance. Simultaneously achieving high piezoelectricity and high softness of organic materials has been one of the most challenges in the field.

To overcome this challenge, we developed a liquid-liquid interface polar engineering to achieve polar (asymmetric) interface by self-assembly of two different linear polymers: polystyrene-block-polyisoprene-block-polystyrene (SIS) and polyethylene glycol (PEG) both with low steric hindrance effect. Due to the big polarity difference between the monomers of two polymers and their inherent low Young's modulus, the constructed PEG/SIS combined film exhibits the merits of high piezoelectricity and high softness. Its longitudinal piezoelectric coefficient is up to 22.9 pC/N overtaking that of most conventional organic piezoelectric materials such as poly(D-lactic acid) (PDLA, ~18.9 pC/N), glycine (~10 pC/N) and cellulose (6.5 pC/N), and is comparable to the performance of PVDF film. Amazingly, this piezoelectricity is uniformly distributed across the whole combined film (12 inch) and can remain 60 days without any attenuation. Besides, the combined film's softness (1×10^{-6} Pa^{-1}) is larger than that of traditional piezoelectric materials such as glycine (~3.3×10^{-11} Pa^{-1}), PDLA (~3.3×10^{-10} Pa^{-1}) and the best PVDF. This technology is expected to provide a direction for the development of organic piezoelectric materials and open up a broad prospect in the field of biomechanical sensing and flexible electromechanical electronics.

Results

Design of piezoelectricity in soft polymers

SIS is a linear block copolymer composed of rigid polystyrene (PS) end blocks and a soft polyisoprene (PI) middle block. The PS end blocks provide the material with necessary mechanical strength, while the PI middle block imparts flexibility and elasticity. Both PI and PEG (polyethylene glycol) lack side chains and have free mobility, which facilitates physical entanglement between them, thereby exhibiting high softness. Additionally, the hydrophobicity of SIS is primarily driven by the PS end blocks, whereas PEG is hydrophilic. This polarity difference readily leads to an uneven distribution of polarity intensity in the combined system (Fig. 1a). To introduce high piezoelectricity into these two soft materials, an asymmetric structure PEG/SIS with high softness was designed to achieve high piezoelectricity in the PEG/SIS combined film. In experiment, the PEG/SIS combined film is synthesized by curing its mixed solution at room temperature (Fig. 1b). Due to the interfacial tension between oil phase and aqueous phase, the toluene solution spread evenly on the water, forming a film as the solvent evaporated (Supplementary Figs. 1–3, Supplementary Note 1). PEG, due to its -O- functional group and terminal hydroxyl group, forms strong electrostatic interactions and hydrogen bonds with water, so it tends to be extracted by the aqueous phase. In contrast, SIS is repelled by the water due to its hydrophobicity. Meanwhile, the entanglement between PEG chains and SIS chains forms a physical cross-linking and thus a network structure, which restricts the movement of PEG and make it difficult to effectively diffuse into the aqueous phase. As a result, during the evaporation of toluene, a phase separation occurs and a clear layered asymmetric structure is constructed due to the polarity difference between PEG and SIS for water, and its diameter exceeds approximately 12 inches, comparable to a standard silicon wafer (Fig. 1c, Supplementary Fig. 2c, Supplementary Note 1).

Asymmetric structure of PEG/SIS combined film

Density functional theory (DFT) is performed to study the interaction between the two monomers (SIS and PEG) in two liquid phases (H_2O and toluene), as shown in Fig. 2a and Supplementary Fig. 4 (Supplementary Note 2). The DFT calculation shows that when the –O– in the PEG molecule interacts with the H_2O molecule, the bond angle (C–O–C) and bond length (–C–O–) of PEG increase accordingly; at the

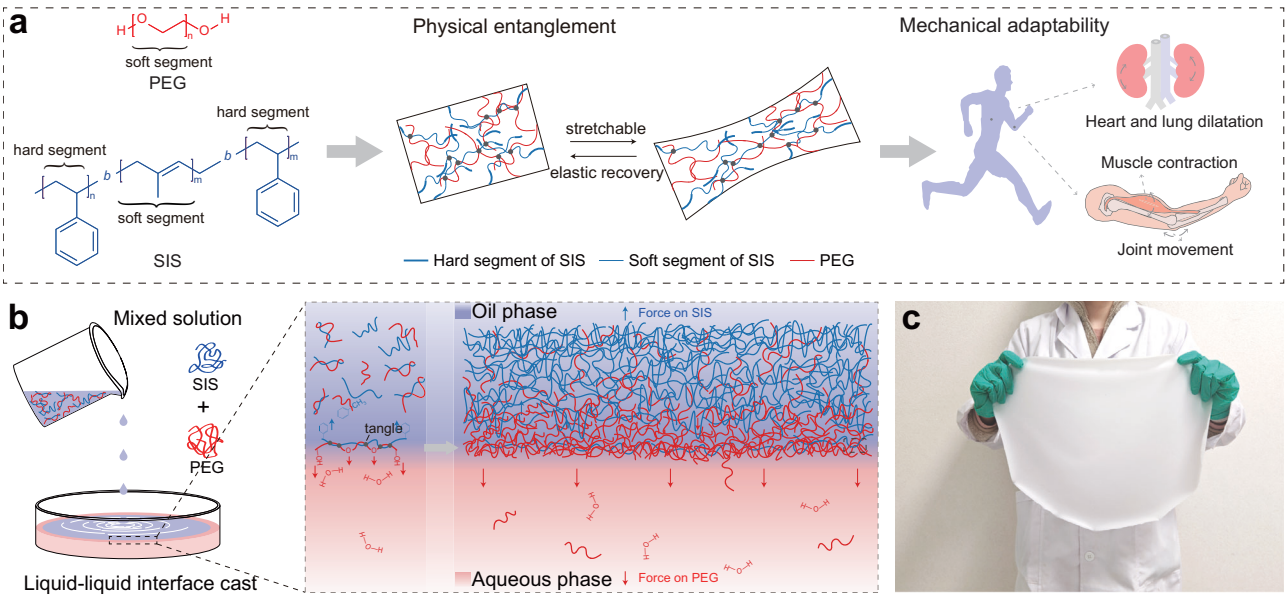

Fig. 1 | Conception and synthesis of piezoelectric soft PEG/SIS combined film. **a** The structures of the two monomers (SIS and PEG), the combined elastic mechanism, and the potential applications in PEG/SIS combined films. **b** Mechanism of polar asymmetric construction. **c** Optical image of the PEG/SIS combined film, whose size is greater than 12 inches.

https://doi.org/10.1038/s41467-025-61526-2

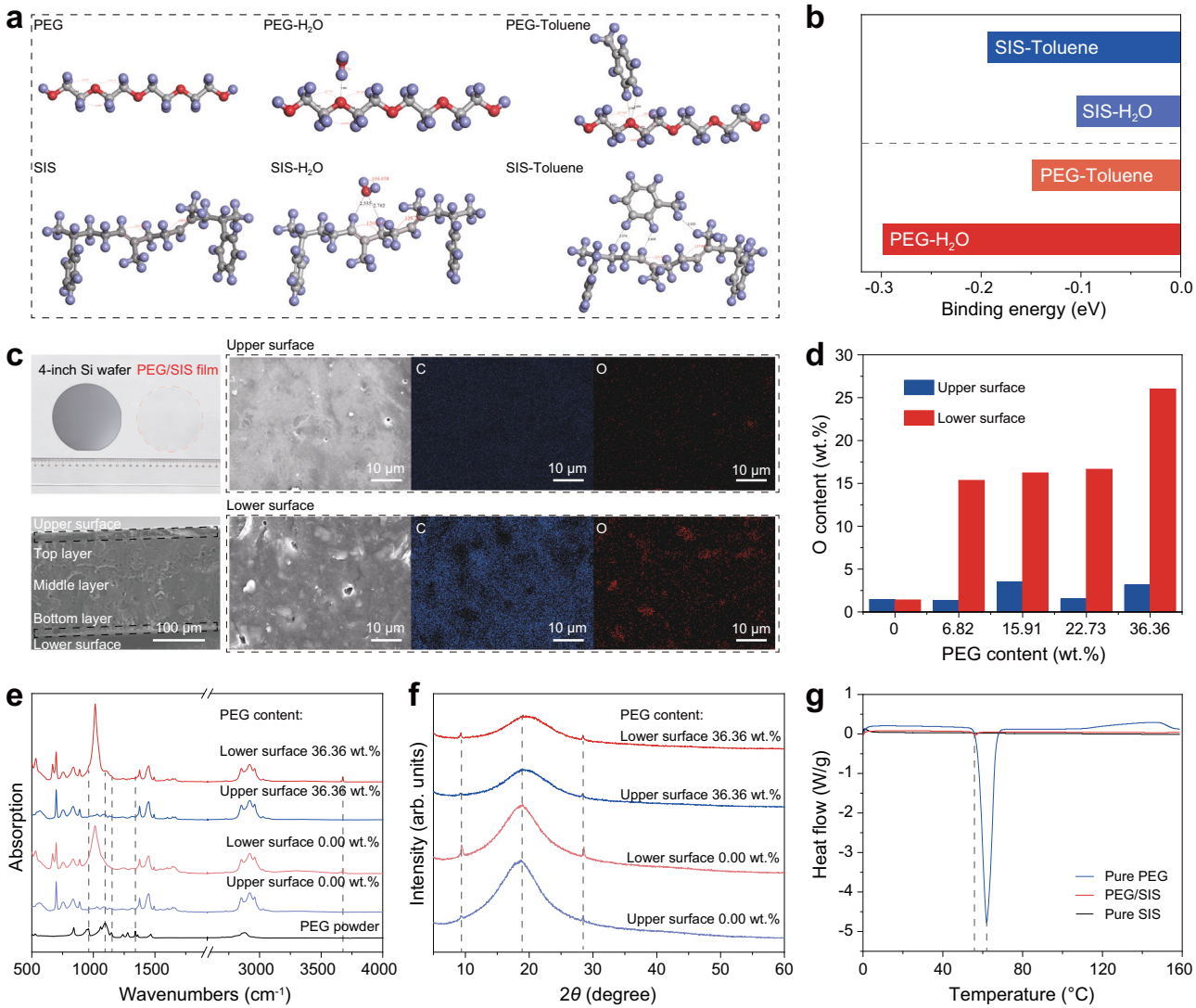

Fig. 2 | Calculation and characterization of PEG/SIS combined film. a Schematics of possible interactions between the two monomers (PEG and SIS) and two reagents (H_2O and toluene). **b** The binding energies calculated by DFT for the four situations (PEG-H_2O, PEG-Toluene, SIS-H_2O, and SIS-Toluene). **c** A number of characteristics of PEG/SIS combined film with 6.82 wt.% PEG content, including the optical picture, the cross-section micro-morphology mapping, and EDS maps of carbon and oxygen atoms on the upper and lower surfaces. **d** Oxygen atom content on the upper and lower surfaces of PEG/SIS combined film with the change of PEG content based on EDS energy spectrum. **e** FTIR spectra of PEG/SIS combined films and pure PEG powders. **f** XRD spectra of PEG/SIS combined films. **g** Heat flow curve of pure PEG powder, PEG/SIS combined film, and pure SIS film.

same time, in the SIS-toluene system, the interaction of the saturated C−C bond also leads to similar changes in the C−C−C bond angle of SIS. In addition, PEG-H_2O and SIS-toluene show higher adsorption energy (Fig. 2b, Supplementary Table 1, Supplementary Note 2). Therefore, in the combined system of SIS and PEG, PEG is more inclined to stay at the liquid-liquid interface and is affected by the interface orientation polarization; in contrast, SIS is more likely to stay within the oil phase, and its dynamics highly shaped by solvent evaporation and the dynamics at the liquid-vapor interface.

Scanning electron microscope (SEM) images show that the PEG/SIS combined film exhibits an obvious layered structure with three layers (bottom layer, middle layer and top layer), as shown in Fig. 2c and Supplementary Fig. 5 (Supplementary Note 3). The bottom layer, situated adjacent to the combined film's lower surface, is affected by the liquid-liquid interface; conversely, the top layer, near the combined film's upper surface, predominantly experiences the influences of solvent evaporation and the liquid-gas interface. The undulating texture of the top layer is predominantly attributed to the irregular and turbulent airflow during the solvent's evaporation process. The middle layer, immersed within the oil phase, is relatively weakly affected by external factors. The total thickness of the three layers is about 200 μm, and the thickness of the bottom layer is much smaller than that of the middle layer and the top layer. There are obvious inconsistencies in the properties and hole distribution of the upper and lower surfaces of the combined film. Energy dispersive spectroscopy (EDS) mapping shows that the oxygen content on the lower surface is much higher than that on the upper surface (Fig. 2d, Supplementary Fig. 6, Supplementary Note 3). As the PEG concentration increases, the oxygen content on the lower surface further increases, while the change on the upper surface is almost negligible. Meanwhile, the carbon content shows the opposite change. These phenomena reveal that the bottom layer and the top layer of PEG/SIS combined film are respectively rich in PEG and SIS, causing the upper and lower surfaces of the combined film to exhibit high polar inhomogeneity. In addition, as the PEG content increases, the hole distribution becomes more obvious, which is mainly due to the increase in PEG concentration weakening the surface tension of water, making it easier for PEG to diffuse into the aqueous phase.

https://doi.org/10.1038/s41467-025-61526-2

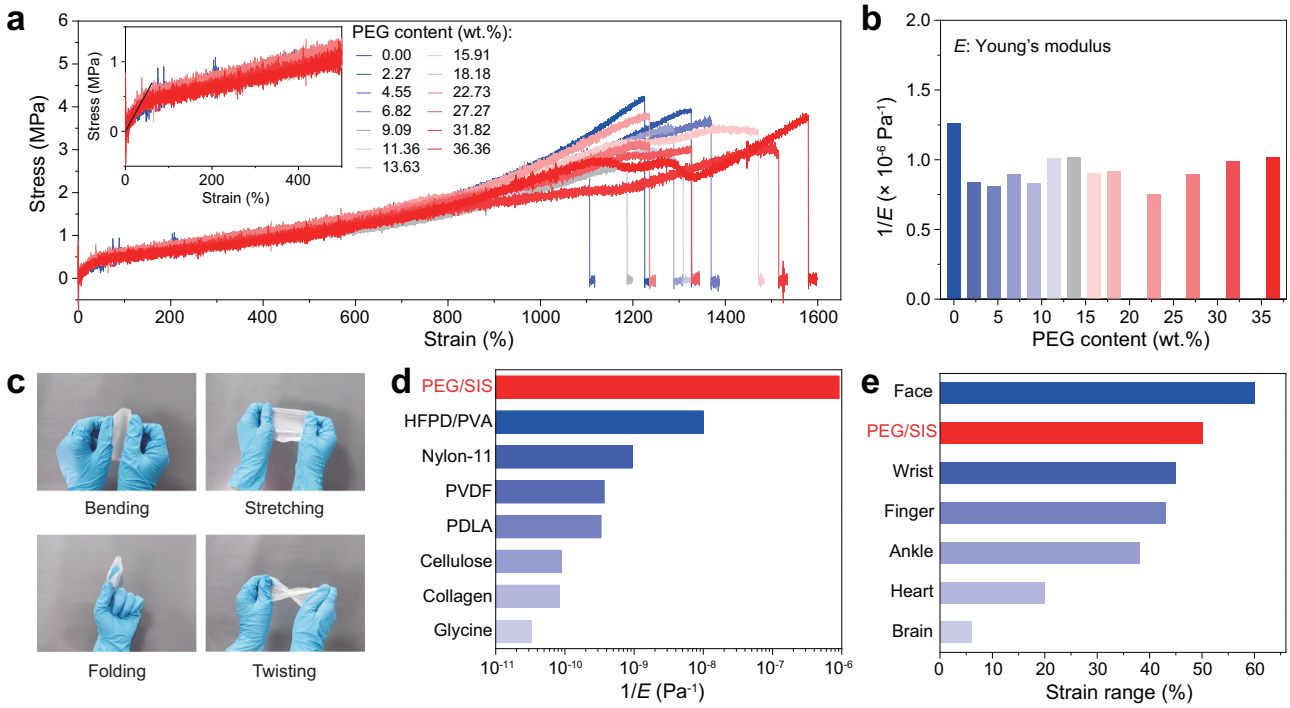

Fig. 3 | Mechanical properties of PEG/SIS combined film. a Stress-strain curves of PEG/SIS combined films with different PEG contents. The inset shows local amplification at low strain of this curve, indicating that these membranes can achieve nearly 50% linear elastic deformation under stress. **b** Softness ($1/E$) of PEG/SIS combined films with different PEG contents calculated by the stress-strain curves in (**a**). **c** Demonstration of PEG/SIS combined films' high softness by bending, stretching, folding and twisting. **d** Comparison of softness between the PEG/SIS combined film and common organic piezoelectric materials. **e** Comparison of strain range between the linear elastic deformation of PEG/SIS combined film and the deformation ranges of biological tissues.

To verify the successful compounding of these two monomers (SIS and PEG), we analyzed the phase transition peaks of monomer PEG, monomer SIS and PEG/SIS combined film in the range of 0–160 °C by differential scanning calorimetry (DSC), as shown in Fig. 2g. The results show that the phase transition temperature of PEG is about 62 °C, while that of PEG in the PEG/SIS combined film decreases to 56.3 °C. This change is attributed to two reasons: Firstly, the existence of SIS weakens the intermolecular van der Waals force of PEG, resulting in a decreased phase transition temperature. Secondly, the entanglement of PEG and SIS hinders the formation of possible ordered crystals, reducing the crystallinity and thus the phase change enthalpy. Therefore, the decrease in phase transition temperature and phase transition enthalpy caused by the addition of SIS indicates that PEG is not completely extracted by aqueous phase, but combined with SIS in the composite system.

To further illustrate the polarity asymmetry of the PEG/SIS combined film, the compositional and structural differences between the upper and lower surfaces of the combined film with different ratios were analyzed by Fourier Transform Infrared Spectroscopy (FTIR) and X-ray Diffraction (XRD). By comparing the FTIR spectra of the upper and lower surfaces of the combined film (Fig. 2e, Supplementary Fig. 7, Supplementary Note 3), it can be seen that the lower surface had obvious absorption peaks at 670 cm^{-1}, 1013 cm^{-1}, and 3678 cm^{-1}. These peaks are related to the out-of-plane bending vibration of –C–H of the SIS benzene ring structure, the stretching vibration of the –C = C– double bond or the deformation vibration of the -C-H bond, as well as the formation of hydroxyl radicals caused by the adsorption of water molecules on the surface. This FTIR difference between upper and lower surfaces of PEG/SIS combined film and pure SIS film reveals that SIS was polarized under the action of the liquid-liquid polar interface. With the addition of PEG, the bending vibration of the –C–O– bond appeared at 960 cm^{-1} on the lower surface of the combined film, and the stretching vibration absorption peaks of –C–O– were observed at 1059 cm^{-1} and 1096 cm^{-1}, respectively, and the stretching vibration absorption peak of –C–O–C– bond was observed at 1340 cm^{-1}. However, these features were not observed on the upper surface of the combined film. This phenomenon indicates that the combined film has formed a layered or gradient structure in the vertical direction. Combined with the results of EDS, it can be concluded that there is a high inconsistency in the polarity of the upper and lower surfaces of the combined film. Commercial SIS is usually amorphous. However, in the XRD data analysis, two weak diffraction peaks of SIS at 9.2° and 28.5° were found, and the intensity of its lower surface was slightly greater than that of the upper surface. With the addition of PEG, the diffraction peak of PEG was not observed, and the diffraction peak intensity of SIS was observed to be weakened. This shows that the entanglement between PEG and SIS weakens their crystallinity (Fig. 2f, Supplementary Fig. 8, Supplementary Note 3). Importantly, these changes indicate that the polar asymmetry of the surface is not affected by the crystallinity of PEG but is closely related to the distribution of the two monomers (SIS and PEG).

Softness of PEG/SIS combined film

Mechanical properties of PEG/SIS combined films with different PEG content were systematically tensile tested in Fig. 3 and Supplementary Fig. 9 (Supplementary Note 4). These films all exhibit breaking elongation up to 1100% (Fig. 3a), fully covering the upper limit of strain produced in biological tissues. Meanwhile, their softness is approximately 1×10^{-6} Pa^{-1} (Fig. 3b), which is much larger than the current organic piezoelectric materials[6,23–25] and composite piezoelectric materials[3] (Fig. 3d), and shows good matches with that of biological tissues such as skin, aorta and cartilage (Supplementary Table 2, and Supplementary Note 4). The combination of high breaking elongation and high softness endows the PEG/SIS combined films advantages for biomedical applications. Notably, despite both SIS and PEG being linear polymers with low steric hindrance, PEG/SIS combined films

consistently exhibit remarkable softness across various blend ratios. This stability is attributed to two synergistic factors: First, the matched segmental dynamics between SIS and PEG enable cooperative stress redistribution to suppress localized hardening. Second, during solvent evaporation, the liquid-phase processing strategy induces topologically confined phase separation, embedding amorphous PEG nanodomains (Fig. 2f) within the SIS matrix (Fig. 3c, Supplementary Fig. 4, Supplementary Note 3). This confinement prevents PEG crystallization and the percolation of rigid phases, ensuring that the soft SIS matrix continues to dominate the overall mechanical response of the material. Unlike the approach of enhancing the softness by PS (Supplementary Fig. 10, Supplementary Note 4), this method provides the possibility to control the polarity difference of the material by adjusting the PEG content while maintaining a high softness. The PEG/SIS combined film can be easily bent, stretched, folded and twisted, demonstrating its ultra-softness (Fig. 3c). This softness is critical for achieving soft, conformable contact with the body's expandable skin, tissues and organs. Generally, the movements of different joints will cause the corresponding skin tissue to deform to varying degrees[8]. For example, the heartbeat can deform cardiac muscle cells by up to 20%; a slight head impact may cause the brain to deform by approximately 6%, as shown in Fig. 3e. It is worth mentioning that these PEG/SIS combined films exhibit good elasticity, and its linear strain capacity can be as high as 50%. This property means that even if the tissue deforms to a considerable extent, the PEG/SIS combined film will not undergo plastic deformation, which enhances its application potential in the field of efficient adaptive biomechanical sensing.

Piezoelectricity of PEG/SIS combined film

To further confirm that the surface polarity asymmetry induces the piezoelectric effect, a laser doppler vibrometer-based atomic force microscopy (AFM) was used to carefully measure and evaluate the microscopic piezoelectricity of PEG/SIS combined films. To ensure that the data obtained indeed reflects the piezoelectricity, the resonance measurement was performed in the voltage ranged from 0 to 5 V to ensure the accuracy and reliability of the measurement results. Figure 4a shows the change of piezo-response amplitude with external voltage in the 1 μm^2 area. It can be seen that the piezo-response amplitude increases with the increase of external voltage and shows good stability and linearity (Fig. 4b). This linear relationship shows that the signal is an inverse piezoelectric signal, that is, the material has piezoelectricity, and its piezoelectric coefficient d_{33} is as high as 8.79 pm/V. The specific test method is shown in Fig. 4c and Supplementary Fig. 11 (Supplementary Note 5).

In order to study the variation of the piezoelectricity of PEG/SIS combined films with PEG concentration, multi-point measurements were performed using a quasi-static d_{33} tester to evaluate the piezoelectricity of PEG/SIS combined films on a small scale (4 inch) (Supplementary Figs. 11, 12, Supplementary Note 5). Additionally, we have conducted macro-scale piezoelectric benchmark tests in the Supplementary Information (Supplementary Fig. 13, Supplementary Note 5) to further validate our results. As shown in Fig. 4d, the piezoelectric coefficient of the pure SIS film is 1.8 pC/N, but as the PEG concentration increases, the piezoelectric coefficient of PEG/SIS combined film increases substantially to a maximum of 22.9 pC/N (average ~13.7 pC/N). This value is comparable to that of the best-performing organic piezoelectric material PVDF. This discovery reveals that although SIS is essentially a non-polar material (Supplementary Fig. 14, Supplementary Note 5), the induced orientation at the liquid-liquid interface will amazingly give it a high piezoelectricity, and the effectiveness of this strategy has been further confirmed in the styrene-maleic anhydride copolymer (SMAC)/SIS film system (Supplementary Figs. 19, 20, Supplementary Note 6). After adding PEG, the material structure shows layered characteristics, and the change in surface chemical composition enhances the polarity of the material, thereby improving the piezoelectricity of combined materials. It is worth noting that PEG/SIS combined films with different ratios can almost show piezoelectricity higher than 7.73 pC/N, which is better than most organic intrinsic piezoelectric materials reported so far, such as collagen (7 pC/N[24]), bone (6 pC/N[26]), cellulose (4.8 ± 1.7 pC/N[25]), etc. Furthermore, by assessing its relative dielectric constant (Fig. 4e) through measuring film's capacitance and thickness (Supplementary Fig. 15, Supplementary Note 5), it can be calculated that the electromechanical coupling factor k_{33} is 0.2%, while the remarkable piezoelectric voltage coefficient g_{33} reaches an impressive 400 V • m/N (Fig. 4f). This value surpasses that of traditional piezoelectric materials such as PZT, BTO, PVDF, etc.[7,27–31], and is comparable to molecular ferroelectrics $(ATHP)_2PbBr_4$[27], $(ATHP)_2PbBr_2Cl_2$[32] and $TMCM_2SnCl_6$[33], as shown in Fig. 4g. These results indicate that a high-voltage signal will be generated by PEG/SIS combined film even under low mechanical stimulation. Notably, the peaks in k_{33} and g_{33} observed at PEG content of 6.82 wt.% and 22.73 wt.% may be related to the transition in the material's microstructure from microphase separation to macroscopic aggregation. At low PEG content (e.g., 6.82 wt.%), the interfacial polarity effect dominates, inducing microphase separation between PEG (polar) and SIS (non-polar). As the PEG content increases, on one hand, the interfacial tension is reduced, allowing PEG to more easily migrate into the aqueous phase; on the other hand, the dipolar interactions among PEG chains become stronger, driving PEG to aggregate and thereby enhancing local polarity. These two factors together lead to a fluctuating composition distribution in PEG/SIS combined films with high PEG content, which can be evidenced by the EDS (Fig. 2d), SEM (Supplementary Fig. 6, Supplementary Note 3), and stress-strain curves (Fig. 3a) of the PEG/SIS combined films. These fluctuations manifest as variations in oxygen content on the upper surface, increased pore size and density, and undulations in stress during yield strength and strain hardening processes. Consequently, a relatively homogeneous structure at low PEG concentrations (<10 wt.%) is more conducive to achieving reliable performance (Fig. 2d, Supplementary Figs. 13, 16, Supplementary Note 5).

To further investigate the temperature dependence of the piezoelectric coefficient of the combined film, the changes in the piezoelectricity of the PEG/SIS combined film (with 6.82 wt.% PEG content) were examined from room temperature to the phase transition temperature range. As shown in Fig. 4h, the d_{33} of PEG/SIS combined film decreases gradually from 21.5 pC/N at 25 °C to 2.7 pC/N at 55 °C (near the PEG phase transition temperature identified by DSC) and ultimately approaches zero at 70 °C (above the melting point of PEG). Furthermore, we investigated the changes in piezoelectricity when the sample was heated to 45 °C (below the phase transition temperature) and then cooled back to room temperature (25 °C), as well as when it was heated to 70 °C and then cooled back to room temperature. The results indicate that within the phase transition temperature range, the sample's d_{33} can recover to around its initial value. However, when the temperature is raised above the phase transition range (e.g., to 70 °C) and then cooled back to room temperature, the d_{33} reaches 3.3 pC/N instead of zero (Supplementary Fig. 17, Supplementary Note 5). These results suggest that the piezoelectricity of the PEG/SIS combined film do not strictly follow the transformation relationship between the paraelectric and ferroelectric phases of traditional ferroelectric materials. The change in piezoelectricity can be attributed to the increased thermal motion of polymer chains at elevated temperatures, which decreases the ability to adsorb charges. Additionally, the melting phase transition of PEG makes it difficult for the material to return to its original state, which also affects the recovery of piezoelectricity to some extent.

In order to study the electromechanical characteristics and stability of PEG/SIS combined films, the frequency dependence of the dielectric and piezoelectricity of the combined films were systematically measured and analyzed. In low-frequency region, the dielectric of PEG/SIS combined films are relatively stable; while in high-frequency

https://doi.org/10.1038/s41467-025-61526-2

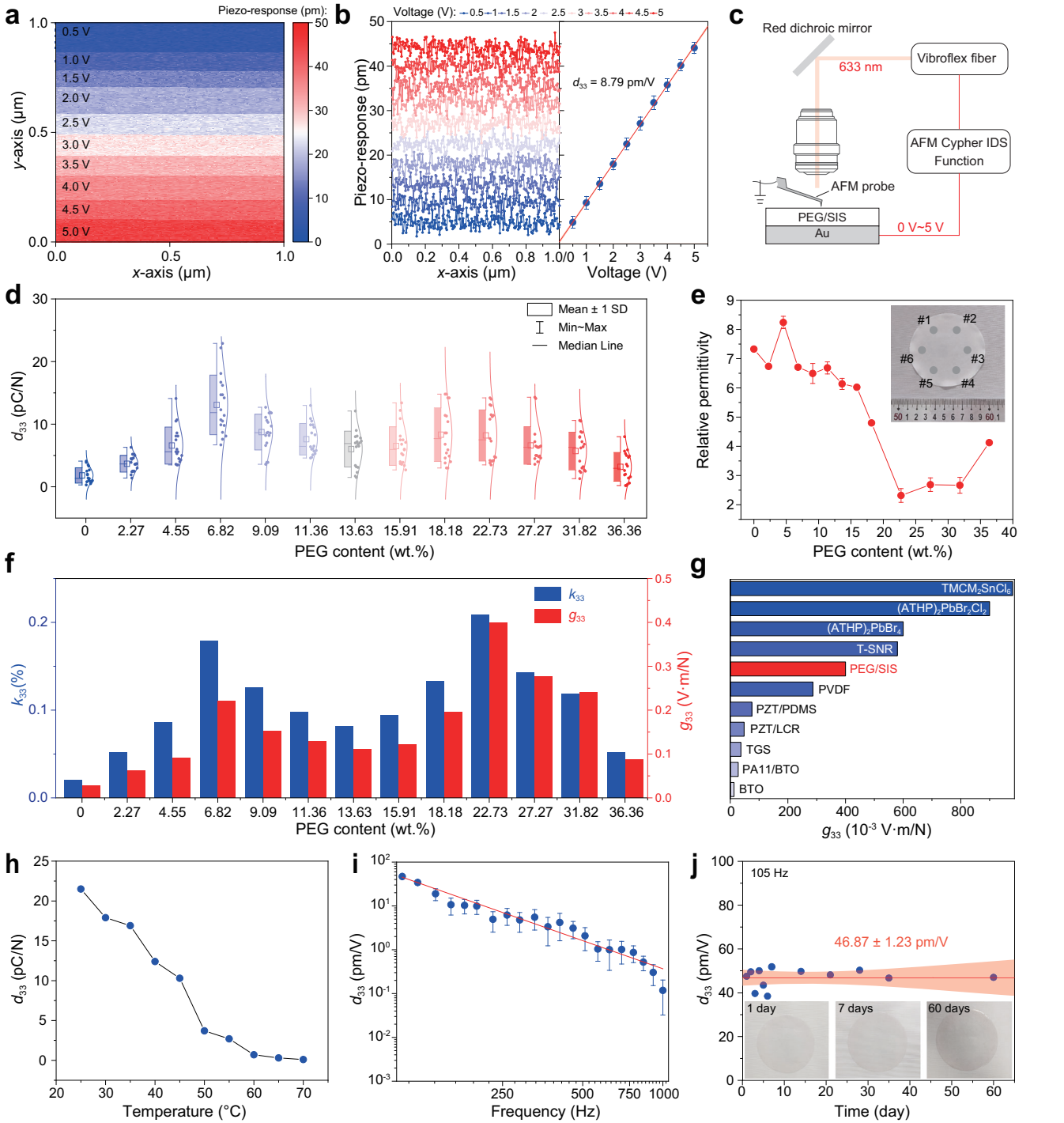

Fig. 4 | Piezoelectricity of PEG/SIS combined film. a Piezo-response of PEG/SIS combined films with different driving voltages. **b** Linear relationship between the piezo-response and the driving voltage. The slope presents the piezoelectric coefficient. Right data presented as mean ± SD, $n = 256$. Data are linearly fitted. **c** Experimental setup for measuring piezo-response of PEG/SIS combined film. **d** The macro-piezoelectricity of PEG/SIS combined films with different PEG contents. Data presented as mean ± SD, $n = 18$. **e** Relative permittivity of PEG/SIS combined films with different PEG contents. The inset shows the positions that measured in the multi-point test. Data presented as mean ± SD, $n = 6$. **f** k_{33} and g_{33} of PEG/SIS combined films with different PEG contents. **g** Comparison of g_{33} between PEG/SIS combined film and common piezoelectric materials. PAII, TGS, LCR, PDMS, and T-SHR represent polyamide 11, triglycine sulfate, polydimethylsiloxane, and the 2,2,6,6-tetramethylpiperidine-1-oxyl oxidation system, respectively. **h** Piezoelectric coefficient of PEG/SIS combined films with 6.82 wt.% PEG content at different temperatures. **i** Piezoelectric coefficient of PEG/SIS combined film with 6.82 wt.% PEG at different frequencies. The dots represent the average piezoelectric coefficients measured at various time points over 60 days, with the relevant data sourced from Supplementary Fig. 18. Data presented as mean ± SD, $n = 12$. Data are linearly fitted. **j** Stability of piezoelectric coefficient of PEG/SIS combined films with 6.82 wt.% PEG content at 105 Hz over 60 days. Data are linearly fitted with a confidence interval of 95% ($P < 0.05$).

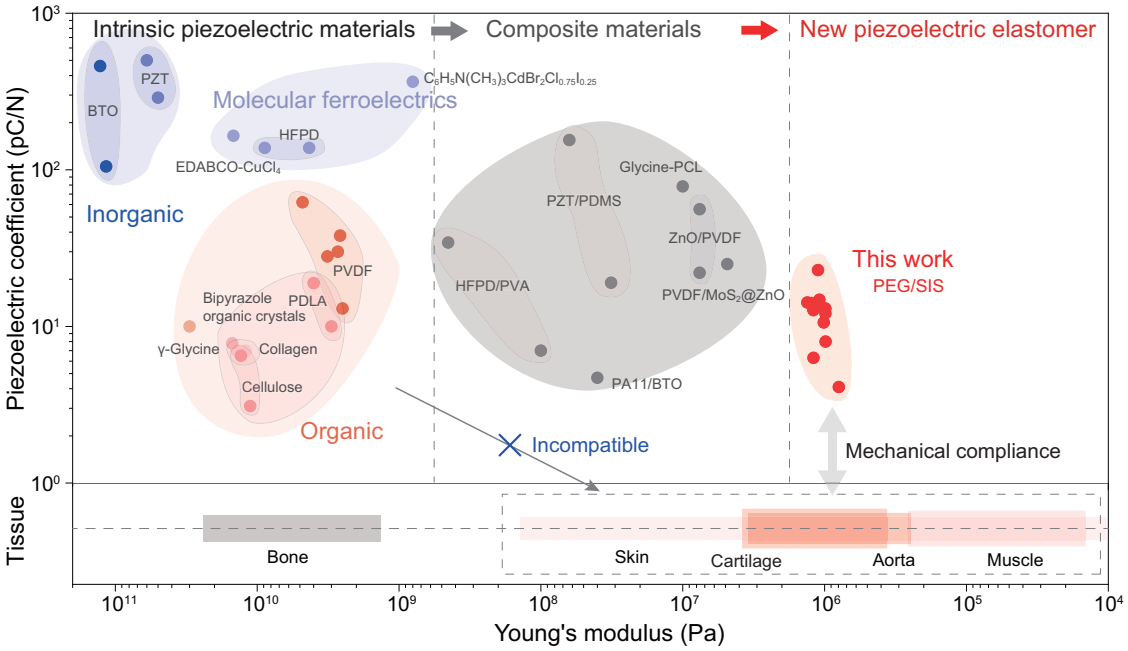

Fig. 5 | Comparison of PEG/SIS combined film with traditional piezoelectric materials. The figure compares the distribution of PEG/SIS combined film and traditional piezoelectric materials in terms of softness and piezoelectricity.

region, the relative dielectric constant is affected by internal polarization, interface effects, and viscoelastic properties, resulting in a change in dielectric response (Supplementary Fig. 15, Supplementary Note 5). Meanwhile, the piezoelectric coefficient decreases with increasing frequency, and eventually tends to a smaller stable value (Supplementary Fig. 18, Supplementary Note 5), which is mainly caused by dielectric loss, indicating that the PEG/SIS combined film has electromechanical response characteristics in low-frequency applications. Moreover, studies on the temperature dependence of piezoelectricity reveal that the PEG/SIS combined film, unlike conventional ferroelectric materials, may not exhibit depolarization. To further investigate this, we conducted long-term tests to assess the piezoelectric stability of the combined film. As shown in Fig. 4i, the frequency dependence of the piezoelectricity of PEG/SIS combined film remains highly consistent over a 60-day testing period, with no signs of degradation. For instance, at a testing frequency of 105 Hz, the piezoelectric coefficient of the combined film remains stable at 46.87 ± 1.23 pm/V over the 60-day period (Fig. 4j). This stability demonstrates the good durability of the PEG/SIS combined film during long-term operation.

Comparison of PEG/SIS combined film with traditional piezoelectric materials. Finally, a comprehensive comparison of piezoelectric constants and softness was conducted among the PEG/SIS combined film and a series of traditional piezoelectric materials, including inorganic piezoelectric ceramics, organic piezoelectric polymers, molecular ferroelectrics, and biomass piezoelectric materials, as well as various composite piezoelectric materials (Fig. 5). It is obvious that the softness of the PEG/SIS combined film is higher than that of existing piezoelectric materials and composite piezoelectric materials. More importantly, it exhibits high piezoelectric performance (22.9 pC/N) within the ultra-high softness range (~ 1×10^{-6} Pa^{-1}), with performance comparable to PVDF (~30 pC/N) and higher than those of glycine (10 pC/N), PDLA (18.9 pC/N)[23], collagen (7 pC/N), and other materials. This finding suggests that the PEG/SIS combined film has great potential, as its high softness is highly compatible with the softness of biological tissues such as skin (7×10^{-9}–2×10^{-4} Pa^{-1}), cartilage (3.2×10^{-7}–6.7×10^{-6} Pa^{-1}), and aorta (2.7×10^{-7}–2.7×10^{-6} Pa^{-1}), etc. This compatible softness makes it an ideal material for manufacturing biomechanical sensors, enabling it to better conform to biological tissue.

Piezoelectric sensors based on PEG/SIS combined films. In view of the good electromechanical conversion performance and long-term stability of PEG/SIS combined film (with 6.82 wt.% PEG content), its application potential in the field of mechanical sensing was further explored, as shown in Fig. 6. Firstly, a PEG/SIS piezoelectric sensor based on the PEG/SIS combined film was prepared based on copper electrodes (Fig. 6a). The sensor exhibited a linear growth relationship between the response voltage and the applied force. Within the stress range of 1.5 to 7.5 kPa, the voltage peak increases quasilinear with the applied force, achieving a sensitivity of ~0.135 V/kPa (Fig. 6b, Supplementary Fig. 21, Supplementary Note 7). Moreover, it can perform stable detection under ultra-low stress (<1.5 kPa), indicating its advantages in the field of biomechanical sensing. Furthermore, by integrating the sensor into wearable devices, real-time monitoring of human multi-joint movements (including the knuckle, elbow, wrist and knee) has been successfully achieved. As shown in Fig. 6c, when the knuckle was gradually bent from 0° (fully extended) to 30°, 60° and 90°, the PEG/SIS piezoelectric sensor produced peak voltages of ~2.11 mV, ~5.44 mV and ~12.17 mV, respectively. Similarly, when the elbow was bent to 30°, 60° and 90°, the response voltage of the sensor is ~4.67 mV, ~6.41 mV and ~13.21 mV, respectively (Fig. 6d). When the PEG/SIS piezoelectric sensor was connected to other joints such as wrist and knee, the peak output voltage was also positively correlated with the bending degree of the joint (Fig. 6e, f). It is worth noting that the voltage signals generated by different joints are specific in terms of amplitude and noise characteristics, which provides a basis for differentiating motion pattern recognition (Supplementary Fig. 21b, Supplementary Note 7). In addition, the sensing system demonstrates good dynamic response capability, capable of clearly distinguishing between rapid movements (~2.6 Hz) and slow movements (~1.4 Hz), as shown in Fig. 6g. With a temporal resolution of ~0.38 s, it is sufficient to meet the needs of continuous motion monitoring.

To further highlight the advantages of high stretchability of PEG/SIS combined film, we further designed a flexible sensor based on

https://doi.org/10.1038/s41467-025-61526-2

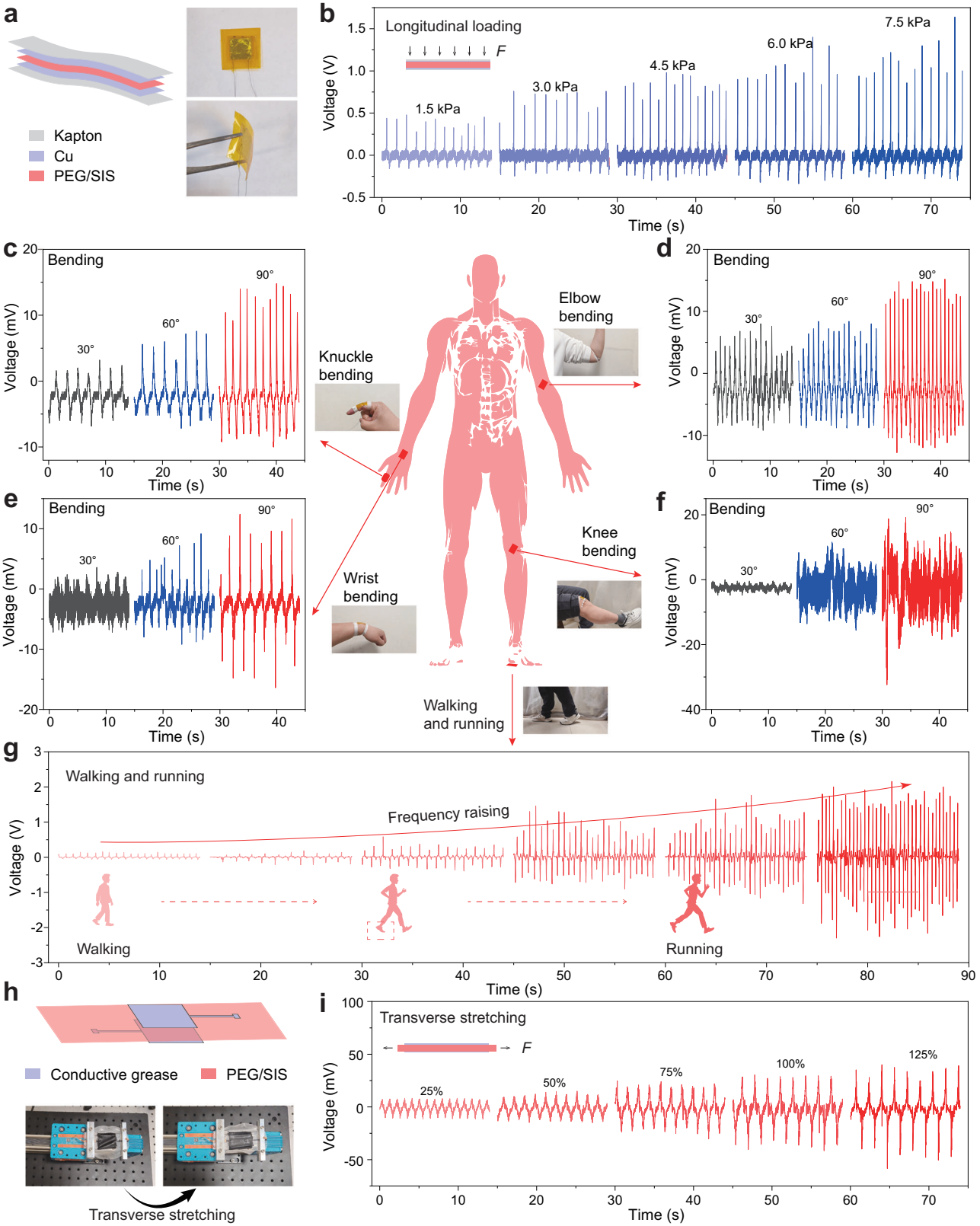

Fig. 6 | Potential applications of PEG/SIS combined film with 6.82 wt.% PEG content for wearable sensor. a–g Demonstration of PEG/SIS piezoelectric sensors for wearable sensing applications. **a** Structural diagram and physical diagram of PEG/SIS piezoelectric sensor. **b** Voltage response of the PEG/SIS piezoelectric sensor under different longitudinal loads. **c–g** PEG/SIS piezoelectric sensor for joint bending monitoring and gait analysis. The sensor is capable of real-time monitoring of bending motions in the knuckles, elbows, wrists, and knees, as well as capturing changes in gait frequency under the sole of the foot. **h**, **i** Schematic diagram, physical diagram, and voltage response of the PEG/SIS piezoelectric sensor under different stretching strains.

conductive grease electrodes (Fig. 6h). Tensile tests showed that within the strain range of 25–125%, the sensor's response voltage was linearly related to the strain (with a sensitivity of ~0.29 mV) (Fig. 6i, Supplementary Fig. 21c, Supplementary Note 7), which covers the typical deformation threshold of biological tissues. So, the PEG/SIS-based sensor, by integrating high sensitivity, broad strain adaptability, and motion-specific detection capabilities, has the potential to establish a quantitative correlation model between electrical signals and mechanical parameters (stress, strain, joint angles). This could thereby provide a possible solution for wearable biomechanical monitoring technology.

Discussion

In summary, this study presents a method of liquid-liquid interface polar engineering for achieving high piezoelectricity in a soft material system. The synthesized PEG/SIS combined film exhibits high piezoelectricity (22.9 pC/N, comparable to PVDF), and the piezoelectricity is almost same throughout the polymer film (>12 inch) and last for 60 days without decay; Meanwhile, its softness (~1×10^{-6} Pa^{-1}) far exceeds that of traditional piezoelectric materials, and is similar to that of the skin, cartilage, and aorta of biological tissues, showing good mechanical compliance. This work contributes to the development of organic piezoelectric materials and benefits to the fields of biomechanical sensing and flexible electromechanical electronics.

Methods

Material preparation

Polystyrene-block-polyisoprene-block-polystyrene (SIS, styrene 17 wt.%) and styrene maleic anhydride copolymer (SMAC, *Mn* ~ 1700) were purchased from Shanghai Macklin Biochemical Technology Co., Ltd. Polyethylene glycol (PEG; Molecular weight 20,000) was supplied from Tianjin Fengyue Chemical Exhibition Co., Ltd. Toluene (GR) was ordered from Chengdu Kelong Chemical Co., Ltd. Polystyrene resin (PS) was purchased from Shanghai Aladdin Biochemical Technology Co., Ltd. All chemicals were used as received.

PEG/SIS combined film synthesis

Firstly, a precise mixture of PEG and SIS heated in a water bath and stirred magnetically was dissolved in a 10 ml toluene solution, separately, with the total mass of solutes set at 1.32 g. After complete dissolution, the mixed solution is subjected to ultrasonic defoaming. Then the mixed solution was carefully poured onto a 10 cm diameter glass petri dish filled with deionized water. After the liquid film is formed evenly, let it stand and let the toluene evaporate naturally in a flowing atmosphere to form a film. Finally, the combined film was collected by soaking it with DuPont paper and dried in a forced-air oven at 35 °C. Additionally, an acrylic container with dimensions of 80 × 60 × 60 cm is used for the synthesis of large-sized films, employing the same process.

DFT calculation

Density functional theory calculations, including a long-range dispersion correction (DFT-D3) as implemented in the Vienna Ab initio Simulation Package (VASP), were employed to predict the interactions between SEG and PEG with H_2O and toluene, respectively. The exchange-correlation functional was represented using the generalized gradient approximation (GGA) in the form of the Perdew-Burke-Ernzerhof (PBE) functional. The projector augmented wave (PAW) method was utilized, with a cutoff energy of 450 eV. The energies were calculated with a convergence accuracy of 1.0×10^{-5} eV. The size of computational cell was 15 × 15 × 30 Å, with a *k*-point set of 5 × 5 × 1 during the calculations. The binding energy between PEG/SIS and Toluene/H_2O, which indicates the interaction between them, was using $E_b = E_{total} - (E_{SIS}/E_{PEG} + E_{Toluene}/E_{H2O})$, where E_{total} is the energy of the supercell containing PEG/SIS and Toluene/H_2O binding together, and E_{SIS}/E_{PEG} and $E_{Toluene}/E_{H2O}$ represent the energies of a single PEG/SIS and Toluene/H_2O molecule, respectively.

General characterization

The thickness of the PEG/SIS combined film is calibrated by a vernier caliper. The material's morphology and energy spectrum information were analyzed by a scanning electron microscopy (Apreo S SEM, Thermo Fisher, America). FTIR and XRD measurements studies were performed independently, with the FTIR analysis executed in the ATR (Attenuated Total Reflectance) mode of the Vertex 70/80 Fourier Transform Mid-Infrared Spectrometer (A531Q1E/Q, Bruker, Germany), and the XRD measurements carried out using the X'pert pro X-Ray Diffractometer (Philips, Netherlands). The heat flow diagram was accurately acquired by a differential scanning calorimeter (DSC 250, Waters, America). The experimental conditions were set to be carried out under an air atmosphere, with the sample subjected to a temperature scan from 0 °C to 160 °C at a controlled heating rate of 10 °C/min.

Elasticity characterization

The stress-strain curve was generated through comprehensive testing on a universal material testing machine (68TM5, INSTRON, America). All PEG/SIS combined films had the same area of 7 mm × 15 mm, and the thickness were measured by a vernier scale.

Piezoelectricity characterization

The microscopic piezoelectricity of the PEG/SIS combined film and its dependence on frequency were quantified using a laser interference multi-physical field sensing imaging system (AFM Cypher IDS, Oxford Instruments, United Kingdom). The macroscopic piezoelectricity of PEG/SIS combined films were measured using a quasi-static piezoelectric coefficient meter (ZJ-6A, Institute of Acoustics, China). The capacitance and dielectric constant of the PEG/SIS combined film were measured and calculated using a 20 mV AC signal with a frequency ranging from 1000 kHz to 5 MHz applied by a semiconductor analyzer (B1500A, Keysight Technologies, America), with the PEG/SIS combined film held between two 0.5 cm × 0.5 cm Au-coated silicon wafers serving as electrodes.

Fabrication of PEG/SIS piezoelectric sensors

To achieve longitudinal stress sensing and wearable applications, the PEG/SIS combined film was cut into a size of 2 cm × 2 cm, with copper foil attached to both surfaces as electrodes, and then it was encapsulated with Kapton tape to form the piezoelectric sensor. For the stretch-sensing application, stretchable sensors were constructed by screen-printing 4 cm × 4 cm conductive grease electrodes (Item No. KLM220713, Kalmar, China) onto both surfaces of the PEG/SIS combined film, and these sensors were directly utilized for tensile testing.

Sensing test

An oscilloscope (DS2202A, RIGOL, China) was used to test the voltage response of the PEG/SIS piezoelectric sensor under longitudinal loading, in vitro experimental conditions, and during cyclic stretching processes. The longitudinal load was applied through finger pressing, and the magnitude of the applied force was precisely evaluated using a force gauge (MCK-Z-I, BENGCHUAN, China). The speed and displacement during the cyclic stretching were achieved using a stretching test platform (TSH-02, Shenzhen Hengyu Laser Instrument Co., Ltd. China). It should be noted that the in vitro stress-sensing experiments were designed and conducted by the first author (Y.K.Z). Informed consent was obtained from all participants involved in the study. Since the experiments did not involve the use of biological tissues or samples derived from humans or animals, ethical approval is not required.

Data availability

DFT data generated in this study are provided in the Supplementary Data 1. Source data are provided with this paper. The data that support the findings of this study are also available from the corresponding author upon request. Source data are provided with this paper.

References

1. Dagdeviren, C. et al. Flexible piezoelectric devices for gastrointestinal motility sensing. *Nat. Biomed. Eng.* **1**, 807–817 (2017).
2. Chen, S. et al. Piezocatalytic medicine: An emerging frontier using piezoelectric materials for biomedical applications. *Adv. Mater.* **35**, 2208256 (2023).
3. Zhang, H.-Y. et al. Biodegradable ferroelectric molecular crystal with large piezoelectric response. *Science* **383**, 1492–1498 (2024).
4. Kim, D. et al. Biomolecular piezoelectric materials: from amino acids to living tissues. *Adv. Mater.* **32**, 1906989 (2020).
5. Jia, N. et al. A wireless ultrasound energy harvester based on flexible relaxor ferroelectric crystal composite arrays for implanted bioelectronics. *Energy Environ. Sci.* **17**, 1457–1467 (2024).
6. Vinogradov, A. & Holloway, F. Electro-mechanical properties of the piezoelectric polymer PVDF. *Fer* **226**, 169–181 (1999).
7. Shepelin, N.-A. et al. New developments in composites, copolymer technologies and processing techniques for flexible fluoropolymer piezoelectric generators for efficient energy harvesting. *Energy Environ. Sci.* **12**, 1143–1176 (2019).
8. Liu, S. et al. Strategies for body-conformable electronics. *Matter* **5**, 1104–1136 (2022).
9. Wang, W. et al. Neuromorphic sensorimotor loop embodied by monolithically integrated, low-voltage, soft e-skin. *Science* **380**, 735–742 (2023).
10. Lee, B.-Y. et al. Virus-based piezoelectric energy generation. *Nat. Nanotechnol.* **7**, 351–356 (2012).
11. Zhang, H.-Y. & Xiong, R.-G. Ferroelectric polymers take a step toward bioelectronics. *Science* **381**, 484–485 (2023).
12. Lovinger, A. J. Ferroelectric polymers. *Science* **220**, 1115–1121 (1983).
13. Chen, X. et al. Relaxor ferroelectric polymer exhibits ultrahigh electromechanical coupling at low electric field. *Science* **375**, 1418–1422 (2022).
14. Ribeiro, C. et al. Electroactive poly(vinylidene fluoride)-based structures for advanced applications. *Nat. Protoc.* **13**, 681–704 (2018).
15. Li, M.-Y. et al. Revisiting the δ-phase of poly(vinylidene fluoride) for solution-processed ferroelectric thin films. *Nat. Mater.* **12**, 433–438 (2013).
16. Shepelin, N.-A. et al. Interfacial piezoelectric polarization locking in printable $Ti_3C_2T_x$ MXene-fluoropolymer composites. *Nat. Commun.* **12**, 3171 (2021).
17. Rat, S. et al. Coupling mechanical and electrical properties in spin crossover polymer composites. *Adv. Mater.* **30**, 1705275 (2018).
18. Yi, J. et al. Water-responsive supercontractile polymer films for bioelectronic interfaces. *Nature* **624**, 295–302 (2023).
19. Qian, X. et al. Fluoropolymer ferroelectrics: Multifunctional platform for polar-structured energy conversion. *Science* **380**, eadg0902 (2023).
20. Lee, J.-W. et al. Robust nanogenerators based on graft copolymers *via* control of dielectrics for remarkable output power enhancement. *Sci. Adv.* **3**, e1602902 (2017).
21. Wang, Z. et al. Bio-inspired mechanically adaptive materials through vibration-induced crosslinking. *Nat. Mater.* **20**, 869–874 (2021).
22. Gao, L. et al. Intrinsically elastic polymer ferroelectric by precise slight cross-linking. *Science* **381**, 540–544 (2023).
23. Yoshida, M. et al. High piezoelectric performance of poly(lactic acid) film manufactured by solid-state extrusion. *Jpn. J. Appl. Phys.* **53**, 09PC02 (2014).
24. Bera, S. et al. Molecular engineering of piezoelectricity in collagen-mimicking peptide assemblies. *Nat. Commun.* **12**, 2634 (2021).
25. Lee, S.-H. et al. Cellulose nanofiber films and their vibration energy harvesting. *Sensors* **22**, 6280 (2022).
26. Fukada, E. & Yasuda, I. On the piezoelectric effect of bone. *J. Phys. Soc. Jpn.* **12**, 1158–1162 (1957).
27. Chen, X.-G. et al. Two-dimensional layered perovskite ferroelectric with giant piezoelectric voltage coefficient. *J. Am. Chem. Soc.* **142**, 1077–1082 (2020).
28. Niu, Q. et al. Silk nanoribbon films with enriched silk II structure and enhanced piezoelectricity for self-powered implantable and wearable devices. *Nano Today* **56**, 102228 (2024).
29. Qi, F., Chen, N. & Wang, Q. Preparation of PA11/$BaTiO_3$ nanocomposite powders with improved processability, dielectric and piezoelectric properties for use in selective laser sintering. *Mater. Des.* **131**, 135–143 (2017).
30. Van Den Ende, D. A., De Almeida, P. & Van Der Zwaag, S. Piezoelectric and mechanical properties of novel composites of PZT and a liquid crystalline thermosetting resin. *J. Mater. Sci.* **42**, 6417–6425 (2007).
31. Babu, I. & De With, G. Highly flexible piezoelectric 0–3 PZT–PDMS composites with high filler content. *Compos. Sci. Technol.* **91**, 91–97 (2014).
32. Khan, A.-A. et al. Superior transverse piezoelectricity in organic-inorganic hybrid perovskite nanorods for mechanical energy harvesting. *Nano Energy* **86**, 106039 (2021).
33. Huang, G. et al. Achieving ultrahigh piezoelectricity in organic–inorganic vacancy-ordered halide double perovskites for mechanical energy harvesting. *ACS Energy Lett.* **6**, 16–23 (2021).

Acknowledgements

This work was supported by the National Natural Science Foundation of China (Nos. 52102173 [Liu], 52472164 [Liu], U21A20175 [Qin]), the Natural Science Foundation of Gansu Province of China (No. 23JRRA1101 [Liu]), and the National Key R & D Project from Minister of Science and Technology (2021YFA1201602 [Qin]).

Author contributions

S.H.L., and Y.Q. supervised the project. Y.K.Z. conceived the idea. Y.K.Z. and S.H.L. designed the investigations. Y.K.Z. performed most of the experiments, and X.N.H., S.Y.Z. and J.L.Z contributed to the experiments. Z.N.Y. performed theoretical calculations. Y.K.Z., X.N.H., H.S, S.H.L., and Y.Q. analyzed the results. Y.K.Z. wrote the initial manuscript. S.H.L. and Y.Q. revised the manuscript. All authors have discussed the results, commented on the manuscript, and approved the final version of the manuscript.

Competing interests

The authors declare no competing interests.

Additional information

Supplementary information The online version contains supplementary material available at https://doi.org/10.1038/s41467-025-61526-2.

Correspondence and requests for materials should be addressed to Shuhai Liu or Yong Qin.

Peer review information *Nature Communications* thanks Joshua Lee and the other anonymous reviewer(s) for their contribution to the peer review of this work. A peer review file is available.